10th International Conference on Fracture Mechanics of Concrete and Concrete Structures
FraMCoS-X
G. Pijaudier-Cabot, P. Grassl and C. La Borderie (Eds)
https://doi.org/10.21012/FC10.232513

EFFECT OF SOFTENING FUNCTION TYPE IN DOUBLE-*K* FRACTURE MODEL: ALKALI-ACTIVATED FLY ASH MORTAR WITH HEMP FIBRES

HANA ŠIMONOVÁ[*], BARBARA KUCHARCZYKOVÁ[*] ZBYNĚK KERŠNER[*], ILDIKÓ MERTA[†], BOJAN POLETANOVIĆ[†], LUCIE MALÍKOVÁ[††] AND STANISLAV SEITL[††]

[*] Brno University of Technology, Faculty of Civil Engineering
Veveří 331/95, 602 00 Brno, Czech Republic
e-mail: simonova.h@vutbr.cz; barbara.kucharczykova@vutbr.cz; kersner.z@fce.vutbr.cz

[†] TU Wien, Faculty of Civil Engineering, Institute of Material Technology, Building Physics and Building Ecology, Research Unit Building Materials and Technology
Adolf-Blamauergasse 1-3, 1030 Vienna, Austria
e-mail: ildiko.merta@tuwien.ac.at; bojan.poletanovic@tuwien.ac.at

[††] Academy of Sciences of the Czech Republic, v. v. i., Institute of Physics of Materials
Žižkova 513/22, 616 62 Brno, Czech Republic
e-mail: malikova@ipm.cz; seitl@ipm.cz

Key words: double-*K* fracture model, softening function, alkali-activation, fly ash, hemp fibre

Abstract: The aim of research reported in this paper is to quantify fracture parameters of selected mortars prepared with an alkali-activated binder and hemp fibres. The alkali-activated materials are environmental friendly building materials, which can be used as an alternative to ordinary Portland cement-based composites. Just like cement-based composites, these materials can be classified as quasi-brittle materials with low energy absorption capacity under tensile load. To enhance the energy absorption capacity, different types of fibres are used in cement-based materials. In this experiment, the hemp fibres were chosen as environmental friendly alternative to the commonly used steel and synthetic materials. The main attention was focused on the evaluation of three-point bending fracture tests of prism specimens, with an initial central edge notch, made of alkali-activated fly ash mortar with different amount of hemp fibres. The load versus crack mouth opening displacement diagrams were recorded during the fracture tests and evaluated using the double-*K* fracture model. This model allows the quantification of two different levels of crack propagation: initiation, which corresponds to the beginning of stable crack growth, and the level of unstable crack propagation. The effect of softening function type and their input parameters on resulting fracture parameters was investigated.

1 INTRODUCTION

Last year, the world production of cement was around 4.1 billion tonnes [1]. Such huge volume of cement production results in very significant environmental impact: total carbon dioxide emissions from the cement industry contribute as much as 8 % of global CO_2 emissions [2].

For that reason, there is an increased effort to develope innovative environmental friendly building materials as an alternative to ordinary Portland cement-based composites. The alkali activated materials (AAMs) belong to a promising alternative to traditional cement-based composites [3, 4]. The use of different secondary-raw materials (metallurgical slags,

coal combustion-based fly ashes, ground granulated blast furnace slag, etc.) or other alumino-silicate materials in AAMs decreases the cement consumption resulting in CO_2 emissions reduction.

Just like cement-based composites, in terms of the overall response, alkali-activated mortars belong to quasi-brittle materials that show what is known as tensile softening, i.e. a gradual decrease in transmitted stress in a significant area ahead of the crack/notch tip. Even a relatively small amount of fibres in mixture can positively affect the resistance of the composite to failure initiation and crack propagation [5−7]. In this paper, the hemp fibres were chosen as the environmental friendly alternative to steel and synthetic materials.

Knowledge of the mechanical and primarily fracture parameters of composites with a brittle matrix is essential for the quantification of their resistance against the crack initiation and propagation as well as for the definition of material models used to simulate the quasi-brittle behaviour of structures made from this type of composites. Therefore, the main attention of this paper is focused on the evaluation of three-point bending fracture tests of prism specimens with an initial central edge notch made of selected fly ash based alkali-activated mortar reinforced with different amount of hemp fibres.

2 MATERIALS AND FRACTURE TESTS

The experimental programme was designed to investigate the effect of different volume percentage of hemp fibres (vol% = 0.5 and 1.0) on the basic mechanical properties and mechanical fracture parameters of the alkali-activated fly ash mortar. For this purpose, the prism specimens with nominal dimensions 40 × 40 × 160 mm were produced.

The power plant fly ash, sodium silicate solution with a modulus of n = 1.91 as alkali activator, river sand with the maximum grain size of 8 mm, water and hemp fibres with length of 10 mm were used to produce the sets of specimens.

The effect of hemp fibres addition was compared with the reference mortar without fibres. Six specimens were made from each mortar; a total number of 18 specimens were tested.

The test specimens were provided with an initial central edge notch before testing and subsequently subjected to the fracture tests in the three-point bending configuration. The nominal depth of notch was about 13 mm and span length was 120 mm. The fracture tests were performed in a very stiff multi-purpose mechanical testing machine. The loading procedure was performed with the requirement of a constant increment of displacement which was set to 0.02 mm/min. In this way, the diagram of loading force F in relation to the crack mouth opening displacement (*CMOD*) during the fracture test was recorded. The *CMOD* value was measured using the extensometer (crack opening displacement transducer), placed between blades which were fixed close to the notch. The extensometer was connected to the HBM Quantum X data logger during the loading test. All measured parameters (time, loading force and crack mouth opening displacement) were continuously recorded into the data logger with a frequency of 5 Hz.

At the beginning of the specimens loading, small-sized fluctuations in the measured values of monitored parameters were recorded. This effect was related to the crushing of small protrusions on the specimen's surface due to the pressure at the support and loading points. These phenomena are usually observed in the short interval just after the beginning of loading test. After this short interval, the *F–CMOD* diagram shows a linear trend. Therefore, it is advisable to correct the beginning part of the measured diagram, in order to obtain the appropriate input values for subsequent diagrams evaluation using selected fracture model. First step is to fit a straight line to data points in the linear part of the diagram, followed by the determination of the intersection of this line with the horizontal axis. The next step is to shift all points of the diagram equidistantly, thus the intersection becomes the origin of the coordinate system.

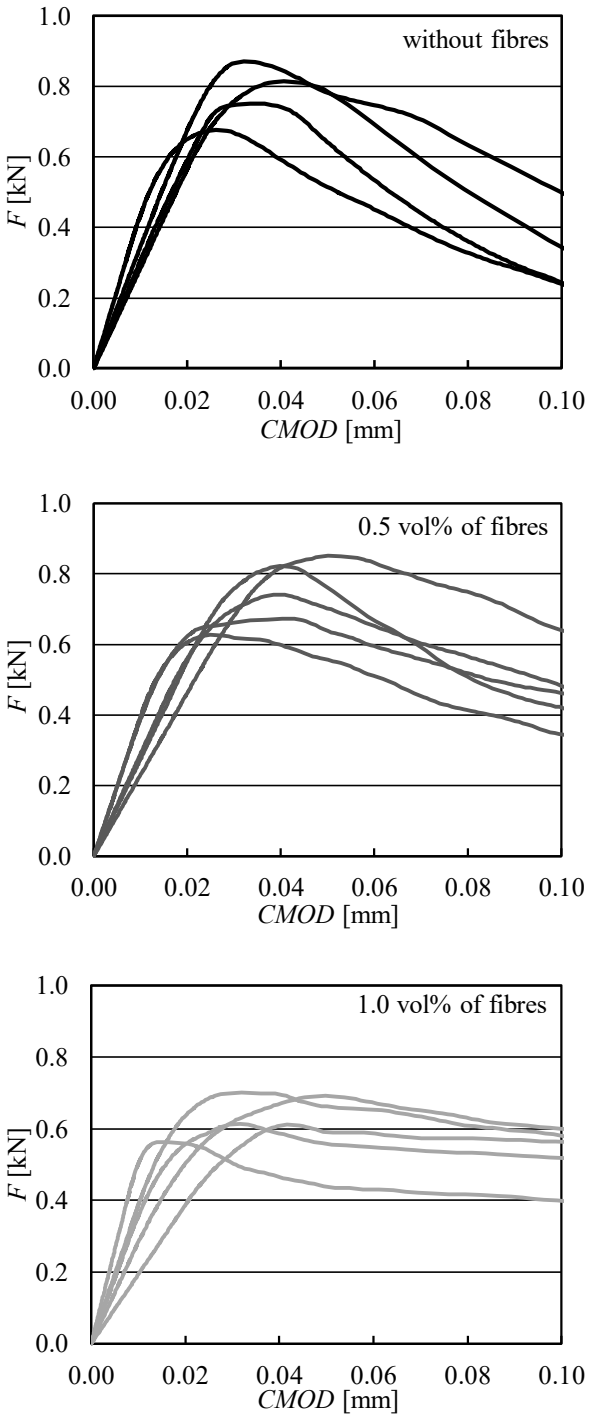

Figure 1: The advanced corrected *F–CMOD* diagrams.

The processing of recorded diagrams including the above-mentioned phenomena was performed using GTDiPS software [8] which is based on the advanced transformation methods for processing of the extensive point sequences. The correction of the measured diagrams in this case included primarily the shifting of the origin of the coordinate system, the smoothing of the diagram and the reduction of the number of points. For this purpose, a chain of transformation steps has been put together into the software. Selected/applicable *F–CMOD* diagrams after the advanced correction are shown in Fig. 1.

3 APPLICATION OF DOUBLE-*K* FRACTURE MODEL

After the above-described processing of the measured diagrams, the obtained *F–CMOD* diagrams were further evaluated using the double-*K* fracture model. The advantage of this model is that the double-*K* fracture criterion can predict the crack initiation, stable crack propagation, and unstable fracture process that occurs during the crack propagation in a quasi-brittle material. According to this criterion, two size-independent parameters, initial cracking toughness K_{Ic}^{ini} and unstable fracture toughness K_{Ic}^{un}, can be used to predict different stages of the fracture process. This model is based on a combination of the concept of cohesive forces acting on the faces of the fictitious (effective) crack increment with a criterion based on the stress intensity factor (details can be found in numerous publications – e.g. in Kumar and Barrai [9]).

In this case, the unstable fracture toughness K_{Ic}^{un} is numerically determined first, followed by the cohesive fracture toughness K_{Ic}^{c}. When both these values are known, the following formula can be used to calculate the initiation fracture toughness K_{Ic}^{ini}:

$$K_{Ic}^{ini} = K_{Ic}^{un} - K_{Ic}^{c}. \quad (1)$$

Details regarding the calculation of both unstable and cohesive fracture toughness can be found in, e.g. [9, 10].

The unstable fracture toughness K_{Ic}^{un} is defined as the critical stress intensity factor, which is similar to effective fracture toughness used in the effective crack model by Karihaloo [11]. Therefore, the well-known linear elastic fracture mechanics formula can be used to determine this parameter, where the peak load F_{max} and corresponding effective crack length a_c are input parameters [9, 10].

To calculate cohesive fracture toughness

K_{Ic}^{c}, the cohesive softening function describing relationship between cohesive stress σ and effective crack opening displacement *COD* needs to be determined first. The cohesive stress $\sigma(CTOD_c)$ at the tip of an initial notch of length a_0 at the critical state can be obtained from this softening curve. In the past, different softening functions was established by many researchers based on the results of extensive experimental studies, including linear [12], bilinear [13, 14], exponential [11, 15] and nonlinear (a product of an algebraic and an exponential term) [16] functions.

In this study, the bilinear softening function according to Petersson [13] was used at first. When using the bilinear softening curve, two cases may occur. In the case I ($CTOD_c \leq COD_s$), the $\sigma(CTOD_c)$ value can be determined according to the formula:

$$\sigma(CTOD_c) = f_t - (f_t - \sigma_s)\frac{CTOD_c}{COD_s}, \quad (2)$$

where f_t is the tensile strength, $CTOD_c$ is the critical crack tip opening displacement, see e.g. [9], σ_s and COD_s are the ordinate and abscissa at the point of slope change of the bilinear softening curve, respectively. According to Petersson [13], the σ_s and COD_s values can be considered using the following expressions:

$$\sigma_s = \frac{1}{3}f_t, \text{ and } COD_s = \frac{2}{9}COD_c, \quad (3)$$

where COD_c is the critical crack opening displacement. In this paper, COD_c is calculated using a value of fracture energy G_F determined via the work-of-fracture method [17] based on measured *F–d* (displacement at the mid-span) diagrams according to this formula:

$$COD_c = \frac{3.6G_F}{f_t}. \quad (4)$$

The tensile strength f_t was firstly estimated using the measured compression strength value f_c using the following relationship [18]:

$$f_t = 0.24f_c^{\frac{2}{3}}, \quad (5)$$

and secondly it was identified from *F–d* diagrams using the artificial neural network based on the inverse analysis method [19, 20].

In the case II ($COD_s \leq CTOD_c \leq COD_c$), the $\sigma(CTOD_c)$ value can be determined according to the formula:

$$\sigma(CTOD_c) = \frac{\sigma_s}{COD_c - COD_s}(COD_c - CTOD_c). \quad (6)$$

To compare the effect of the type of softening function on double-*K* fracture model parameters, the nonlinear softening function according [16] was also considered as follows:

$$\sigma(CTOD_c) = f_t\left\{\left[1 + \left(c_1\frac{CTOD_c}{COD_c}\right)^3\right]\exp\left(-c_2\frac{CTOD_c}{COD_c}\right) - \frac{CTOD_c}{COD_c}(1 + {c_1}^3)\exp(-c_2)\right\} \quad (7)$$

where c_1 and c_2 are the material constants, which were taken according to [16] as $c_1 = 3$ and $c_2 = 6.93$.

In the case of nonlinear softening function, COD_c is calculated according to this formula:

$$COD_c = \frac{5.136G_F}{f_t}. \quad (8)$$

Finally, the value of the load F_{ini} is determined according to the formula (9). This value can be defined as the load level at the beginning of stable crack propagation from the initial crack/notch:

$$F_{ini} = \frac{4 \cdot W \cdot K_{Ic}^{ini}}{S \cdot F_1(\alpha_0) \cdot \sqrt{a_0}}, \quad (9)$$

where W is the section modulus (determined as $W = 1/6 \cdot B \cdot D^2$), B and D are the width and depth of the specimen, respectively; S is the span length, $F_1(\alpha_0)$ is the geometry function for a three-point bend beam [11] and α_0 is the a_0/D ratio.

Table 1 introduces the input values used for determination of parameters of softening functions which was used for the calculation of fracture parameters via double-*K* fracture model.

For illustration, Figs. 2 and 3 show the difference between the types of used softening function and the effect of input parameters on their shape. Fig. 2 introduces the bilinear softening functions according to [13], the tensile strength was estimated based on the measured values of compressive strength using Eq. (5).

Fig. 3 introduces the nonlinear softening functions according to [16], the tensile strength was identified from *F–d* diagrams using the

artificial neural network based on the inverse analysis method [19, 20].

Table 1: Input parameters used for determination of softening functions parameters; mean values (coefficient of variations).

Parameter	Unit	Content of fibres [vol%] 0	0.5	1.0
G_F	[J/m^2]	44.0 (27.7)	71.4 (29.3)	133.9 (20.8)
f_c	[MPa]	29.7 (5.0)	29.9 (4.0)	27.1 (3.2)
$f_{t,\text{ based on }fc}$	[MPa]	2.30 (5.0)	2.31 (4.0)	2.16 (3.2)
$f_{t,\text{identified}}$	[MPa]	4.11 (20.5)	3.16 (22.6)	1.96 (10.0)

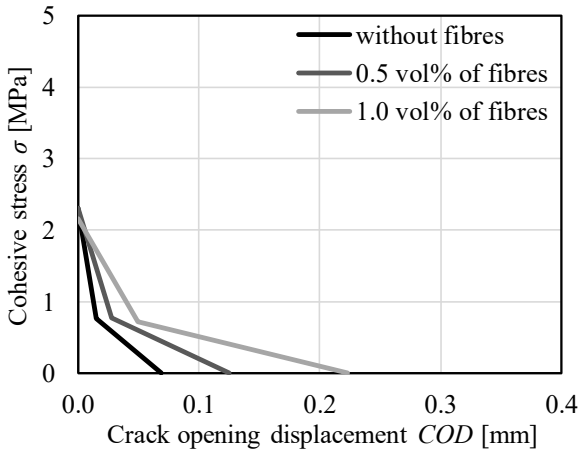

Figure 2: Used bilinear softening functions according to [13] for alkali-activated mortars with different amount of hemp fibres.

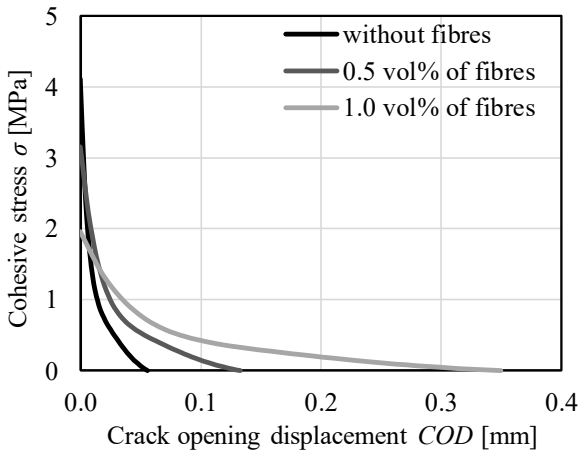

Figure 3: Used nonlinear softening functions according to [16] for alkali-activated mortars with different amount of hemp fibres.

4 RESULTS

The results obtained from the measured *F–CMOD* diagrams using double-*K* fracture model are introduced in Tables 2 and 3: the unstable fracture toughness K_{Ic}^{un}, the $K_{Ic}^{ini} / K_{Ic}^{un}$ ratio, i.e. the ratio expressing the resistance to stable crack propagation, the maximum load F_{max}, the F_{ini} / F_{max} ratio, i.e. the ratio between the load level at the beginning of the stable crack propagation and the maximum load obtained during the test, and the critical crack opening displacement COD_c.

The Tables 2 and 3 summarize the values obtained using the bilinear and nonlinear softening function, respectively. Based on the results shown in Table 2 it can be stated that the value of unstable fracture toughness is not significantly influenced by addition of hemp fibres into the alkali-activated matrix. The maximum load decreases slightly with addition of hemp fibres in amount of 1 vol%.

Table 2: Mean values of selected parameters (coefficients of variations); the bilinear softening function was used.

Parameter	Unit	Content of fibres [vol%] 0	0.5	1.0
K_{Ic}^{un}	[MPa·m$^{1/2}$]	0.463 (10.8)	0.505 (12.1)	0.475 (17.8)
F_{max}	[kN]	0.732 (13.3)	0.727 (12.9)	0.649 (6.6)
Tensile strength estimated based on measured values of compressive strength				
$K_{Ic}^{ini} / K_{Ic}^{un}$	[−]	0.626 (11.9)	0.559 (22.2)	0.501 (15.9)
F_{ini} / F_{max}	[−]	0.742 (7.3)	0.693 (12.9)	0.643 (14.1)
COD_c	[mm]	0.068 (24.3)	0.125 (23.4)	0.223 (20.2)
Tensile strength identified from *F–d* diagrams				
$K_{Ic}^{ini} / K_{Ic}^{un}$	[−]	0.398 (17.3)	0.451 (11.2)	0.544 (14.3)
F_{ini} / F_{max}	[−]	0.472 (14.4)	0.565 (4.6)	0.696 (7.7)
COD_c	[mm]	0.039 (19.1)	0.093 (31.3)	0.245 (19.0)

Table 3: Mean values of selected parameters (coefficients of variations); the nonlinear softening function was used.

		Content of fibres [vol%]		
Parameter	Unit	0	0.5	1.0
Tensile strength estimated based on measured values of compressive strength				
K_{Ic}^{ini} / K_{Ic}^{un}	[−]	0.630 (11.6)	0.573 (20.9)	0.516 (15.1)
F_{ini} / F_{max}	[−]	0.748 (6.9)	0.712 (11.6)	0.663 (13.7)
COD_c	[mm]	0.098 (24.3)	0.178 (23.4)	0.318 (20.1)
Tensile strength identified from *F–d* diagrams				
K_{Ic}^{ini} / K_{Ic}^{un}	[−]	0.403 (16.7)	0.460 (9.4)	0.557 (13.4)
F_{ini} / F_{max}	[−]	0.477 (13.6)	0.577 (5.7)	0.722 (7.9)
COD_c	[mm]	0.055 (19.3)	0.133 (31.4)	0.350 (19.0)

The resistance to stable crack propagation, in this case expressed by K_{Ic}^{ini} / K_{Ic}^{un} ratio is changing with the addition of hemp fibres. The type of softening function has no significant effect on the absolute values. However, the way of determination of the tensile strength influences the absolute value of investigated parameters which has an important effect on the results obtained from both softening functions. If the tensile strength estimated based on the measured value of compressive strength is used in evaluation, the resistance to stable crack propagation decreases by about 10 and 20 % with addition of 0.5 % and 1.0 % of hemp fibres, respectively.

On the contrary, if the tensile strength identified from *F–d* diagrams is used, the effect of addition of hemp fibres is opposite. The resistance to stable crack propagation increases by about 15 and 40 % with addition of 0.5 % and 1.0 % of hemp fibres, respectively.

The same trend was also observed in the case of F_{ini} / F_{max} ratio.

5 CONCLUSIONS

The conclusions can be divided into two parts: one part related to the effect of the type of applied softening function on the calculated values of investigated characteristics and second part related to the assessment of the influence of the addition of hemp fibres on the behaviour of particular mortars. Based on the presented results it can be stated that the type of softening function has no significant effect on the calculated values of fracture parameters for all investigated mortars. In this case, the input parameters of softening functions are more important, especially the way of estimation of tensile strength. Commonly, the compressive strength values are used for estimation of the tensile strength of the materials. Therefore at first, the tensile strength was estimated based on the empirical relation, which is implemented in ATENA software [18]. Based on this relation, material parameters of model are defined and used to simulate the behaviour of structures made from the specific quasi-brittle material.

More appropriate is to determine the tensile strength directly from the tensile test performed in the configuration most similar to the loading of the real structural element. The tensile strength was identified herein from the measured *F–d* diagrams. The artificial neural network based on the inverse analysis method [19, 20] was used to obtain a more accurate value. Presented results showed high significance of the absolute value of tensile strength especially in the case of determination of the material resistance to the stable crack propagation. The two different ways of tensile strength estimation gave different absolute values of this parameter which provided two diametrically different results of the resistance to stable crack propagation of investigated mortars.

The resistance to unstable crack propagation expressed here by the unstable fracture toughness is not significantly influenced by addition of hemp fibres into the alkali-activated matrix. On the contrary, the alkali-activated mortars with hemp fibres expressed a much better post-peak behaviour with a better load carrying capacity in comparison with the reference composite.

ACKNOWLEDGEMENTS

The support of project No. 8J18AT009 and project No. 18-12289Y is gratefully acknowledged.

REFERENCES

[1] U.S. Geological Survey, 2018. *Mineral commodity summaries*. U.S. Geological Survey.

[2] Andrew, R.M., 2018. Global CO_2 emissions from cement production. Earth Sys. Sci. Data **10**:195–217.

[3] Scrivener, K.L., John, V.M.C. and Gartner, E.M., 2016. *Eco-efficient cements: Potential, economically viable solutions for a low-CO_2 cement-based materials industry*. United Nations Environment Programme, Paris.

[4] Shi, C., Krivenko, P. and Roy, D., 2006. *Alkali-Activated Cements and Concretes*. CRC Press, Taylor & Francis group.

[5] Johnston, C.D., 2010. *Fiber-reinforced Cements and Concretes*, Taylor & Francis.

[6] Smarzewski, P., 2019. Influence of basalt-polypropylene fibres on fracture properties of high performance concrete. *Compos. Struct*. **209**:23–33.

[7] Kizilkanat, A.B., et al. 2015. Mechanical properties and fracture behavior of basalt and glass fiber reinforced concrete: An experimental study. *Constr. and Build. Mater.* **100**:218–224.

[8] Frantík, P. and Mašek, J., 2015. *GTDiPS software*, http://gtdips.kitnarf.cz/

[9] Kumar, S. and Barai, S.V., 2011. *Concrete Fracture Models and Applications*. Springer.

[10] Zhang, X. and Xu, S., 2011. A comparative study on five approaches to evaluate double-*K* fracture toughness parameters of concrete and size effect analysis. *Eng. Frac. Mech.* **78**:2115–2138.

[11] Karihaloo, B.L., 1995. *Fracture mechanics and structural concrete*. Longman Scientific & Technical

[12] Hillerborg, A., Modeer, M. and Petersson, P.E., 1977. Analysis of crack formation and crack growth in concrete by means of fracture mechanics and finite elements. *Cement Concr. Res.* **6**:773–782.

[13] Petersson, P.E., 1981. *Crack growth and development of fracture zone in plane concrete and similar materials*. Report No. TVBM-1006, Division of Building Materials, Lund Institute of Technology, Lund, Sweden.

[14] Wittmann, F.H., Rokugo, K., Brühwiler, E., Mihashi, H. and Simopnin P., 1988. Fracture energy and strain softening of concrete as determined by compact tension specimens. *Mater. Struct*. **21**:21–32.

[15] Gopalaratnam, V.S. and Shah, S.P. 1985. Softening response of plain concrete in direct tension. *J. Am. Concr. Inst.* **82**:310–323.

[16] Reinhardt, H.W., Cornelissen, H.A.W. and Hordijk, D.A., 1986. Tensile tests and failure analysis of concrete. *J. Struct. Engng.* **112**:2462–2477.

[17] RILEM TC-50 FMC Recommendation, 1985. Determination of the fracture energy of mortar and concrete by means of three-point bend test on notched beams. *Mater. Struct.* **18**:285–290.

[18] Červenka, V., Jendele, L. and Červenka, J. 2012. ATENA Program documentation – Part 1: theory. Červenka Consulting, Prague.

[19] Novák, D. and Lehký, D., 2006. ANN Inverse Analysis Based on Stochastic Small-Sample Training Set Simulation.

Eng. Appl. Artif. Intell. **19**:731–740.

[20] Lehký, D., Keršner, Z. and Novák, D., 2014. FraMePID-3PB Software for Material Parameters Identification Using Fracture Test and Inverse Analysis. *Adv. Eng. Softw.* **72**:147–54.